


**Large anomalous Hall angle in the Fe<sub>60</sub>Al<sub>40</sub> alloy induced by substitutional atomic disorder**J. Kudrnovský, V. Drchal, and F. Máca *Institute of Physics, Czech Academy of Sciences, Na Slovance 2, CZ-182 21 Praha 8, Czech Republic*I. Turek *Institute of Physics of Materials, Czech Academy of Sciences, Žitkova 22, CZ-616 62 Brno, Czech Republic*

S. Khmelevskiy

*Center for Computational Materials Science, Institute for Applied Physics, Vienna University of Technology, Wiedner Hauptstrasse 8, A-1040 Vienna, Austria* (Received 30 September 2019; revised manuscript received 27 January 2020; accepted 11 February 2020; published 26 February 2020)

The electronic and transport properties of the ordered B2-(Fe<sub>60</sub>Al<sub>40</sub>) phase which undergoes a continuous transition into the disordered A2-(Fe<sub>60</sub>Al<sub>40</sub>) phase are studied from first principles. The disordering is characterized as a gradual interchange of atoms between Fe and Al sublattices under the condition that the total amount of Fe and Al atoms is kept unchanged. This is the simplest model of gradual disordering of the ordered phase due to the ion irradiation. The physical properties are strongly influenced by varying local environment of Fe atoms on both sublattices. This leads to the transition between a high moment at large disorder and a very low moment in the ordered phase. Similar behavior is found also for anomalous Hall conductivity and anomalous Hall angle. Unusual behavior of the longitudinal conductivity as a function of degree of disorder is due to the shift of the Fermi level of majority states from the *sp*-like part to the *d* states with increasing ordering. The disordered phase has a large anomalous Hall angle as contrasted with a negligible anomalous Hall angle for well ordered samples, which is in agreement with recent experiment.

DOI: [10.1103/PhysRevB.101.054437](https://doi.org/10.1103/PhysRevB.101.054437)**I. INTRODUCTION**

Many properties of metallic alloys such as magnetic and transport ones can be tuned by varying the atomic order in the alloy. A typical example is the order-disorder transition induced by the varying temperature. Disordered phase usually exists at high temperature while annealing at lower temperature can lead to a formation of various ordered structures. On the contrary, the ordered phase turns into a disordered one at the order-disorder temperature on heating. This order-disorder phenomenon is well established (see, e.g., Ref. [1]). However, there exist also other tools of changing the ordered phase into the disordered one without thermal treatment, namely, the ball milling [2], cold working [3], high-pressure compression [4], and ion irradiation [5].

Ion-beam irradiation with low fluences is a very effective tool for the creation of different atomic and magnetic structures in a controlled way. Variation of the irradiation fluence and ion energy allows one to vary magnetic properties continuously as contrasted with chemical disorder which influences the magnetic ordering on a microscopic scale. In fact, ion-beam irradiation creates chemical disorder in films of different thicknesses. An intensively studied system is the B2-Fe<sub>60</sub>Al<sub>40</sub> alloy with CsCl structure which can be turned into a disordered A2-Fe<sub>60</sub>Al<sub>40</sub> one with a bcc structure (see, e.g., Ref. [6] and references therein). Chemical disorder is due to vacancies created by Fe and Al atoms knocked from their

initial positions in ordered B2-alloy by ions. These vacancies are subsequently filled back by thermal diffusion giving a disordered alloy with varying degree of disorder depending on the characteristics of the irradiation beam.

Recently, a systematic study of B2 and A2 phases of Fe<sub>60</sub>Al<sub>40</sub> alloy was done [6] in which a clear evolution of the local environment around Fe atoms and Fe orbital polarizations in alloy films has been observed. Results of experiment are supported by theoretical study of densities of states (DOS), averaged spin magnetic moments, and distributions of Fe-Fe nearest neighbors (NN) in both phases. It should be noted that B2-(Fe<sub>60</sub>Al<sub>40</sub>) alloy is paramagnetic and thermodynamically stable at room temperatures while the disordered phase is a ferromagnetic and metastable one. The ordered B2 phase of Fe<sub>60</sub>Al<sub>40</sub> is nonstoichiometric with some amount of antisite Fe[Al] atoms on the native Al sublattice of the ideal B2-FeAl lattice. The whole process of disordering is thus quite complex and its quantitative description is a challenge for the theory. In the present study we attempt to simulate this process on the first-principle level in the simplest possible way, namely, as a gradual interchange of Fe and Al atoms under the condition that the total amount of Fe and Al atoms is kept unchanged.

We will evaluate properties of the alloy that depend on the degree of disorder on the quantitative, first-principle level including also transport properties. In particular, in addition to conventional conductivity, we will evaluate spin-orbit induced transport properties among them in the first place the

TABLE I. Calculated Fe  $d$  moments (in  $\mu_B$ ) averaged over all lattice sites in ordering B2-(Fe<sub>60</sub>Al<sub>40</sub>) alloy for  $S = 0.0$  (bcc) and  $S = 1.0$  are compared with corresponding values in Ref. [6] obtained using SQS and KKR (Korringa-Kohn-Rostoker)-CPA approaches.

$S$	SQS	KKR-CPA	Present
0.0	1.420	1.391	1.254
1.0	0.553	0.539	0.589

anomalous Hall conductivity and a closely related anomalous Hall angle. We will demonstrate that local Fe environment plays a decisive role in the understanding of variation of studied quantities such as the total and local Fe moments, longitudinal conductivity, and anomalous Hall conductivity/angle due to the degree of disorder in the sample. We have found an unusually large value of the anomalous Hall angle (for metallic alloys with such small spin-orbit coupling) reaching 3% for the disordered A2 phase in agreement with a recent experiment [7]. This large value should be contrasted with a negligible anomalous Hall angle in the ordered B2 phase, which shows the importance of disorder.

## II. FORMALISM

### A. Structure

We consider the B2 structure formed by two interpenetrating simple cubic sublattices occupied by Fe and Al atoms. Gradual interchange of Fe and Al atoms between the sublattices while keeping the numbers of Fe and Al atoms constant allows us to interpolate continuously between the maximally ordered B2 phase and the fully disordered A2 alloy. Such interchange of atoms is called the antisite Fe-Al disorder and can be characterized by the long-range order (LRO) parameter  $S$ . Total energy estimates (see Table II below) indicate that such antisite disorder is energetically favorable. We thus consider the nonstoichiometric B2-(Fe<sub>1-x</sub>Al<sub>x</sub>)-(Al<sub>0.8-x</sub>Fe<sub>0.2+x</sub>) alloy, where  $0 \leq x \leq 0.4$  and define the LRO parameter as  $S = 1 - 2.5x$ . The limiting cases of maximally ordered B2 phase ( $S = 1$ ) and disordered A2 phase ( $S = 0$ ) correspond to  $x = 0$  and  $x = 0.4$ , respectively. We note that alternative definitions of the LRO parameter  $S$  exist for nonstoichiometric alloys according to which the state of maximal order is described by  $S$  smaller than 1. In the disordered phase both sublattices are equally occupied by 60% of Fe and 40% of

TABLE II. Formation energies of possible defects (in eV) calculated for B2-FeAl ordered alloy by the VASP [16,17] using supercell containing 54 atoms and thus corresponding to the defect concentration of 3.7%. Defect  $X$  on the sublattice  $Y$  is denoted as  $X[Y]$ . The PBE exchange-correlation potential was employed [22].

Defect	Unrelaxed	Relaxed
Fe[Al]	0.76	0.68
Al[Fe]	1.23	0.56
Vac[Fe]	1.02	0.77
Vac[Al]	3.35	2.35

Al atoms (bcc lattice as a doubled simple cubic lattice). In the partially ordered state the first sublattice (called here the native Fe sublattice) is occupied by Fe and Al atoms that form an alloy Fe<sub>1-x</sub>Al<sub>x</sub>. The second sublattice (called here the native Al sublattice) is occupied by Fe and Al atoms in the proportion corresponding to the Fe<sub>0.2+x</sub>Al<sub>0.8-x</sub> alloy. This description represents a simplified model of the disordering process which, nevertheless, captures several important features, namely, Fe and Al antisites as a source of disorder and the presence of a continuous transition from ordered to disordered phases. This gradual transition allows us to understand better the disordering process than the study of the final B2 and A2 phases only. Moreover, this model is suitable for an assessment of the interplay between the local environments around Fe atoms (characterized by the average number of the nearest-neighbor Fe atoms) and the studied magnetic and transport properties. On the other hand, short-range order effects are neglected in this model. We note that it is impossible to relate the LRO parameter  $S$  to irradiation fluence characteristics on a quantitative level.

### B. Electronic structure and transport

The spin-polarized electronic structure calculations were done using the Green function formulation of the tight-binding linear muffin-tin orbital (TB-LMTO) method in the atomic sphere approximation (ASA) while the alloy disorder is described by the coherent potential approximation (CPA) [8]. Specifically, we employ both the scalar-relativistic and relativistic (Dirac) versions of the TB-LMTO method. In both cases the exchange-correlation potential of Vosko, Wilk, and Nusair (VWN) [9] and the *spd*-basis set were used. We assume the model of collinear Fe spins. This is a reasonable assumption as the dominating Fe-Fe interactions are usually ferromagnetic and the moments are collinear at low temperatures; see, e.g., Ref. [10]. Calculated self-consistent alloy potentials are then used as an input for transport calculations.

The transport properties are described by the conductivity tensor  $\sigma$  with components  $\sigma_{\mu\nu}$  ( $\mu, \nu = x, y, z$ ). The resistivity tensor  $\rho$  with components  $\rho_{\mu\nu}$  is obtained simply by inversion of the conductivity tensor  $\rho = \sigma^{-1}$ . We assume that the magnetization is pointing along the  $z$  axis. The conductivity tensor is determined in the framework of the Kubo-Bastin (KB) formulation of the fully relativistic transport in disordered magnetic alloys which includes both the Fermi-surface and Fermi-sea terms on equal footing [11]. The Fermi-surface term contains contribution only from the states at the Fermi energy and includes the most important elastic scattering effects due to impurities. The Fermi-sea term, on the contrary, depends on all occupied states below the Fermi energy; this term contributes only to the antisymmetric part of the tensor  $\sigma_{\mu\nu}$ . In chosen cases we also employ the scalar-relativistic transport counterpart determined in the framework of the Kubo-Greenwood (KG) approach (only diagonal elements of  $\sigma_{\mu\nu}$  are nonzero in the present cubic system) [12,13]. Once the transport tensor is determined, the average value of diagonal elements of  $\sigma_{\mu\nu}$  gives the longitudinal conductivity, the anomalous Hall conductivity (AHC) is given by the off-diagonal element  $\sigma_{xy}$ , while the anomalous Hall angle  $\alpha_H$  is defined as the ratio  $\sigma_{xy}/\sigma_{xx}$ . We also determine the anisotropic

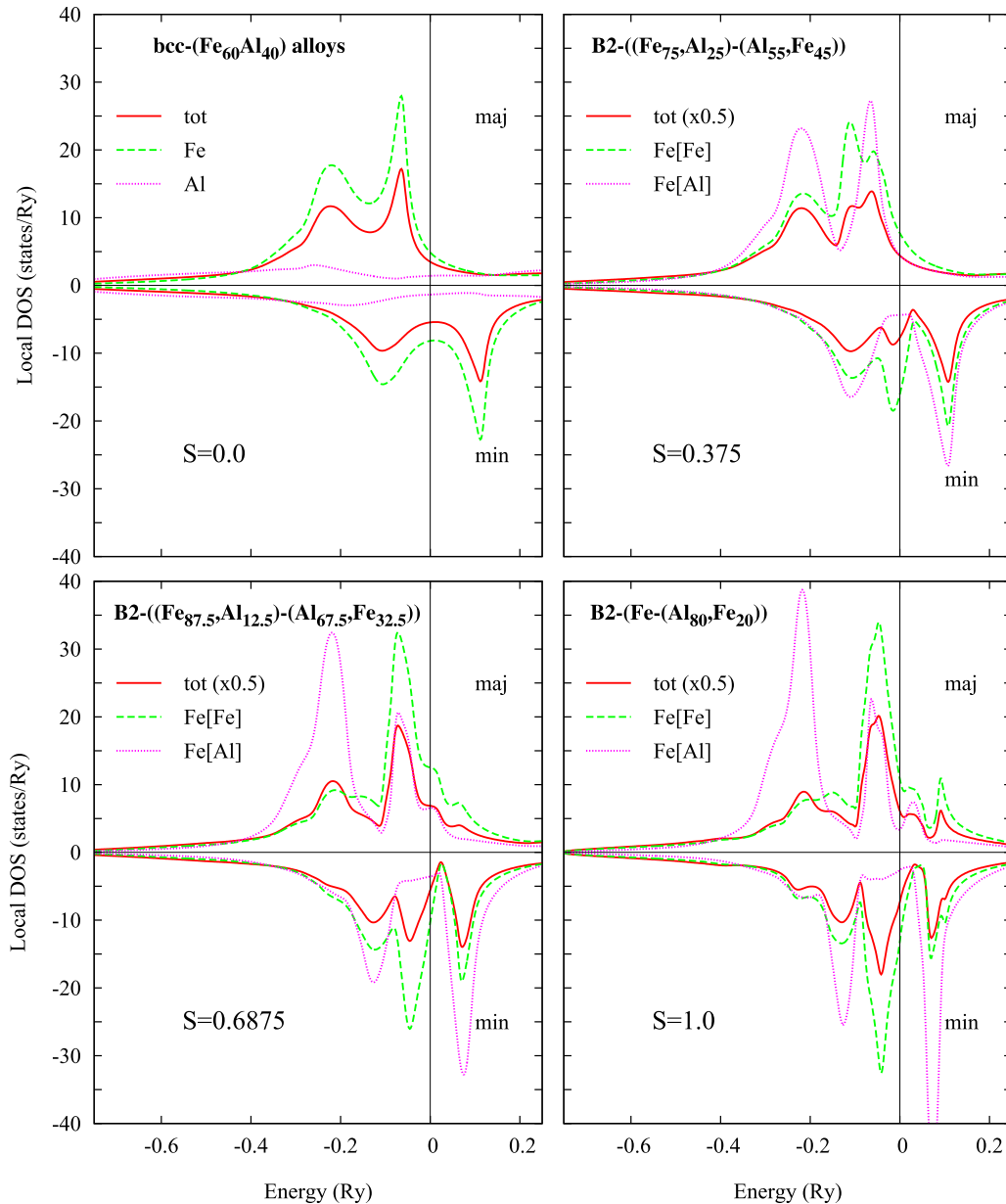


FIG. 1. Relativistic spin-resolved total densities of states (DOS) and the local Fe densities of states (LDOS) on the native Fe lattice (Fe[Fe]) as well as antisite Fe-LDOS on the native Al lattice (Fe[Al]) for ordering B2-(Fe<sub>60</sub>Al<sub>40</sub>) alloys and different values of the LRO parameter  $S$ . Total LDOSs are scaled by a factor 0.5 to fit bcc-unit cell. (a)  $S = 0$  corresponding to the disordered bcc-(Fe<sub>60</sub>Al<sub>40</sub>) alloy. In this case Fe[Fe] and Fe[Al]-LDOS coincide. We show also Al-LDOS in this case. (b)  $S = 0.375$  corresponding to B2-(Fe<sub>75</sub>Al<sub>25</sub>)-(Al<sub>55</sub>Fe<sub>45</sub>). (c)  $S = 0.6875$  corresponding to B2-(Fe<sub>87.5</sub>Al<sub>12.5</sub>)-(Al<sub>67.5</sub>Fe<sub>32.5</sub>). This alloy corresponds to the lowest/largest conductivity/resistivity; (d)  $S = 1.0$  corresponding to the maximally ordered B2-(Fe-(Al<sub>80</sub>Fe<sub>20</sub>)) alloy.

magnetoresistance AMR defined as  $AMR = (\rho_{zz} - \rho_{xx})/\rho_{tot}$ , where  $\rho_{tot}$  is the average value of diagonal components of the resistivity tensor.

### III. RESULTS

#### A. Electronic structure

To illustrate the underlying electronic structure, we show in Fig. 1 the total and Fe-resolved densities of states for ordering B2-(Fe<sub>60</sub>Al<sub>40</sub>) alloys with different values of the LRO parameter  $S$ . We note that the majority LDOSs are narrower than the minority ones. This is due to the fact that minority levels

are energetically above majority ones and are thus less bound by the alloy potential. The total DOS exhibits a similar trend as the local Fe[Fe]-LDOS on its native lattice. On the contrary, the antisite Fe[Al]-LDOS has large splitting of majority and minority components which is almost independent of  $S$ . The majority and minority states behave differently with increasing  $S$ : The Fermi level gradually merges into the  $d$  band for majority states while for minority states it is inside the  $d$  band for any value of  $S$ . This fact will influence the behavior of conductivity as a function of order (see below). Finally, present DOSs for  $S = 0.0$  and  $S = 1.0$  calculated in the framework of the CPA agree reasonably well with a recent study [6] based

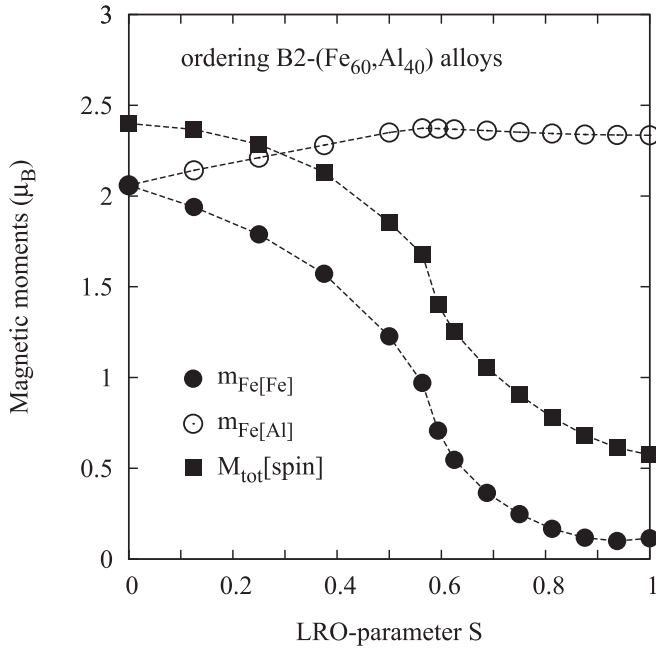


FIG. 2. Total averaged spin moments (per two-site unit cell) and local Fe moments of ordering B2-(Fe<sub>60</sub>Al<sub>40</sub>) alloys as a function of the LRO parameter  $S$ . We show both the native Fe moments on the Fe sublattice ( $m_{\text{Fe[Fe]}}$ ) and the antisite Fe moments on the Al sublattice ( $m_{\text{Fe[Al]}}$ ).

on the supercell-SQS (special quasirandom structure) which includes also possible local environment effects.

In Fig. 2 we illustrate magnetic properties of ordering B2-(Fe<sub>60</sub>Al<sub>40</sub>) alloys as a function of the LRO parameter  $S$ . We find that the moments of antisite Fe[Al] atoms are large and weakly dependent on  $S$ . Their large values are related to the bcc-like Fe NN environment of Fe[Al] antisites (for  $S = 1.0$  each Fe[Al] atom is surrounded by eight Fe NN atoms). Note that native and antisite moments coincide for  $S = 0.0$  (bcc-random alloy is treated as two equivalent sublattices in B2 structure). The behavior of moments of native Fe[Fe] atoms is quite different. We observe a steep continuous transition from the high moment state for small  $S$  values to a very low moment (about  $0.1\mu_B$ ) for large values of  $S$ . The transition from high to low moment occurs for  $S \approx 0.6$ . Dominating Fe atoms on native Fe sublattice (Fe[Fe] atoms) have mainly Al atoms in the first NN coordination shell and Fe atoms only in the second NN shell for large  $S$ . Negligible moments of Fe[Fe] atoms are compatible with the fact that stoichiometric B2-FeAl is nonmagnetic. There exist contradictory explanations of this fact in the literature [14,15]. For  $S = 0.0$  and  $S = 1.0$  we can compare our results with those in Table III of Ref. [6]. The moments are given in Table I and we find a good agreement between our results and those of Ref. [6]. The dependence of the total averaged spin moment on the LRO parameter  $S$  essentially follows the dependence of the dominating native Fe[Fe] moments. Finally, we observe a well-known fact that the ordered B2 phase exhibits a pronounced ferromagnetism due to chemical disordering [6].

The steep continuous transition of native Fe[Fe] moments from the high to low spin state mediated by increasing order

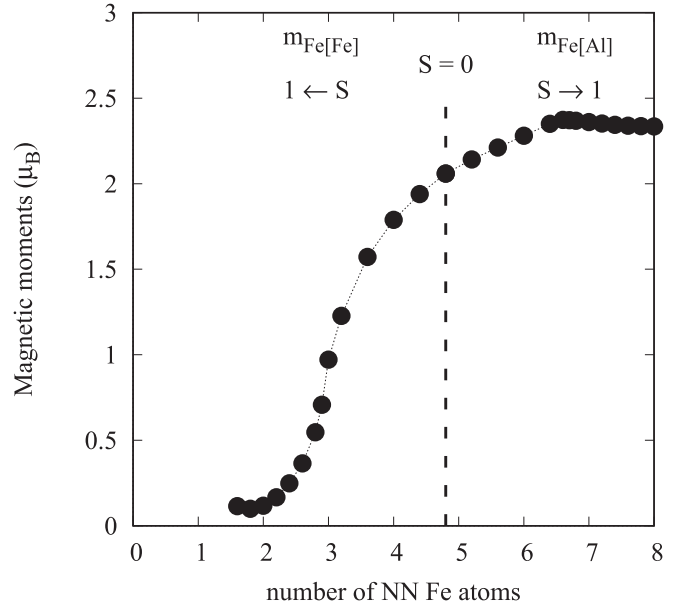


FIG. 3. Local Fe moments on the native Fe sublattice ( $m_{\text{Fe[Fe]}}$ ) and the antisite Fe moments on the Al sublattice ( $m_{\text{Fe[Al]}}$ ) as a function of the averaged number of nearest-neighbor (NN) Fe atoms. The dashed vertical line corresponds to  $S = 0.0$ , where  $m_{\text{Fe[Fe]}}$  and  $m_{\text{Fe[Al]}}$  coincide and where each atom has the same number (4.8) of NN Fe atoms. The LRO parameter  $S$  increases to  $S = 1.0$  both to the left ( $m_{\text{Fe[Fe]}}$ ) and to the right ( $m_{\text{Fe[Al]}}$ ) giving thus different numbers of NN Fe atoms for a given  $S > 0.0$ . The number of NN Fe atoms for  $S = 1.0$  on the native Fe sublattice (Fe[Fe]) is 1.6 and on the Al sublattice (Fe[Al]) is 8.

is an important fact and it deserves more attention. We have mentioned above qualitative relation between high/low moments of native Fe[Fe] atoms and composition of the first NN coordination shell. Magnetic moments on Fe atoms for alloys with a partial order between the limits  $S = 0$  and  $S = 1$  are shown in Fig. 3 as a function of the average number of their NN Fe atoms. A simple estimate is based on the assumption of a random distribution of NN Fe atoms on both sublattices. In the alloy B2-(Fe<sub>1-x</sub>Al<sub>x</sub>)-(Al<sub>0.8-x</sub>Fe<sub>0.2+x</sub>), where  $0 \leq x \leq 0.4$ , the numbers of NN Fe atoms are  $1.6 + 8x$  for Fe[Fe] and  $8 - 8x$  for Fe[Al] atoms. The calculated averaged number of NN Fe atoms for  $S = 0.0$  is the same for native and antisite atoms and it equals 4.8. On the other hand, for the ordered sample ( $S = 1.0$ ) we obtain two different values, namely, 1.6 for Fe[Fe] atoms and 8 for Fe[Al] atoms. The average over all Fe atoms is 2.67. These results agree with those in Ref. [6]. Of course, in more general numerical simulations fluctuations around these ideal values exist as seen in Ref. [6]. The experiment gives for an averaged number of NN Fe atoms the values 5 ( $S = 0.0$ ) and 3.47 ( $S = 1.0$ ). Agreement is very good for the disordered sample and worse for the ordered one, which may indicate the presence of some disorder in the ordered sample due to its preparation. We note a continuous transition between high and low moments. In particular, the high-to-low moment transition occurs for a Fe NN number between 2.6 and 2.8 corresponding to  $S$  around 0.6–0.7.

The last point is related to one possible mechanism causing the order-disorder transition. In the present study we model

disordering in terms of Fe-Al swaps which turn the originally ordered phase into the disordered one. It is important to know the formation energies of possible defects which we have calculated using the Vienna ab initio simulation package (VASP) supercell approach [16,17]. Here we employ the simplest possible approach in which the formation energy FE of a defect is defined as  $FE = E_{\text{tot}}[\text{def}] - E_{\text{tot}}[\text{id}] - \sum_i n_i E_i$ , where  $E_{\text{tot}}[\text{def}]$  and  $E_{\text{tot}}[\text{id}]$  are total energies of the supercells with (def) and without (id) defects,  $n_i$  indicates the number of atoms of type  $i$  ( $i = \text{Fe, Al, vacancy}$ ) that have been added to ( $n_i > 0$ ) or removed from ( $n_i < 0$ ) the supercell when the defect is formed, and  $E_i$ 's are total energies of atoms in their most probable bulk phase. We consider as defects also vacancies (Vac) which can be formed, e.g., due to ion bombardment. Results are summarized in Table II. Formation energies of Fe[Al], Al[Fe], and vacancies on Fe are reasonably small, in particular, the relaxed ones. The effect of relaxation is particularly strong for Al[Fe] due to the larger Al atomic size while for Fe[Al] it is small. For vacancies the relaxation is also important and we note a very large formation energy for vacancies on Al. The Fe-Al swap is formed by two single defects, namely by Fe[Al] and Al[Fe] and for low swap concentration a reasonable estimate is the sum of their formation energies. It is interesting to compare such energy with that determined by the CPA. We assume as a reference state the maximally ordered state and as a perturbed system the alloy with 2.5% of Al[Fe] antisites, i.e., the alloy B2-(Fe<sub>97.5</sub>Al<sub>2.5</sub>)-(Al<sub>77.5</sub>Fe<sub>22.5</sub>). The estimated formation energy 1.94 eV agrees well with the unrelaxed value calculated by the VASP, but, as expected, it is larger than the relaxed one. It should be noted that the above values should be taken with care as they assume an equilibrium state while the disordered phase is a metastable one.

The present model yields the DOSs and magnetic moments in a reasonable agreement with the experiment and more demanding numerical SQS simulations. We therefore expect that corresponding self-consistent potentials can be used also as an input for transport calculations below.

Finally, we note that the B2-(Fe<sub>60</sub>Al<sub>40</sub>) alloy is paramagnetic and thermodynamically stable at room temperature and can be transformed into a ferromagnetic metastable disordered phase by various methods (ball milling, cold working, high-pressure compression, or ion irradiation). Our theoretical approach similar to that of Ref. [6] is formulated at  $T = 0$  K and as pointed out in the Introduction our aim is to investigate the effect of gradual disordering on various transport properties, while details of thermodynamics are beyond the scope of the present paper.

### B. Longitudinal conductivity

The longitudinal conductivity is the simplest transport property and it is given by the diagonal elements of the conductivity tensor. Results are summarized in Fig. 4, where we show, in addition to the  $xx$  component of the relativistic conductivity, also its scalar-relativistic counterpart and its decomposition into the spin-resolved contributions. The effect of spin-orbit coupling is weak and both relativistic and scalar-relativistic conductivities are very similar. The decomposition of the relativistic conductivity into spin-resolved contributions

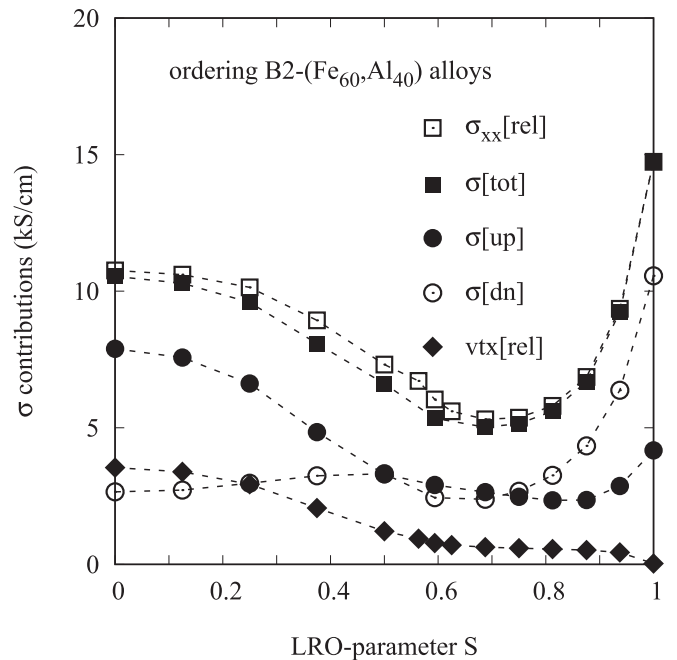


FIG. 4. Conductivity of ordering B2-(Fe<sub>60</sub>Al<sub>40</sub>) alloys as a function of the LRO parameter  $S$ : Relativistic conductivity  $\sigma_{xx}[\text{rel}]$  (empty boxes), total scalar-relativistic conductivity  $\sigma[\text{tot}]$  (filled boxes), and its decomposition into majority  $\sigma[\text{up}]$  (filled circles) and minority  $\sigma[\text{dn}]$  (empty circles) contributions. Finally, by filled diamonds are shown the transport vertex corrections, i.e., the vertex corrections to the Fermi-surface term. Note that for the present cubic case all nonzero scalar relativistic components of conductivity tensor are equivalent to the total conductivity.

is generally impossible due to the channel mixing by the spin-orbit coupling but in the present case the effect is very small and one can employ such decomposition also for the interpretation of relativistic results. For alloys with small spin-orbit coupling relativistic effects are pronounced if the conductivity in one channel strongly dominates (e.g., in fcc-NiFe [18]). In the present case (Fig. 4) the contributions of both spin channels are comparable, i.e., the disorder in both channels is stronger than the spin-orbit effect. We note that the dependence of the conductivity on the ordering is unexpected. While larger conductivity for the ordered case as compared to the disordered one and its smaller values with decreasing  $S$  close to  $S = 1.0$  are expected due to increasing disorder, the conductivity minimum close to  $S = 0.7$  which is a consequence of the increase of the conductivity with decreasing  $S$  close to  $S = 0$  is unexpected.

In order to understand the change of the total conductivity with  $S$  it is instructive to analyze its individual spin-resolved contributions. While the behavior of the minority contribution  $\sigma[\text{dn}]$  is expected as it essentially increases with increasing order, the behavior of majority contribution  $\sigma[\text{up}]$  is responsible for unusual behavior of the total conductivity. With the exception of large values of  $S$  (where it also increases)  $\sigma[\text{up}]$  is a decreasing function of  $S$  up to about  $S = 0.8$ . This can be explained using Fig. 1. The Fermi level of majority states lies for small values of  $S$  in the  $sp$ -like part of spectra as contrasted with minority states where it is in the  $d$ -band complex for any

value of  $S$ . This is the reason for much higher conductivity of majority states as compared to minority ones for small  $S$ . But with increasing  $S$  the  $d$ -band complex of majority states is gradually shifted to the Fermi level and consequently the majority contribution to the conductivity decreases due to the stronger scattering by  $d$  states as compared to the  $sp$  ones. The majority conductivity weakly increases with  $S$  only close to  $S = 1.0$  due to a high order in the alloy. The behavior of total conductivity as a function of  $S$  is given by the competition between the increasing minority component and the decreasing majority component of the conductivity resulting in a minimum of the total conductivity at  $S = 0.6875$ . Note that this value of  $S$  marks also the transition from high- to low-spin states for native Fe atoms as well as for the total spin moment. The increase of total conductivity with increasing degree of disorder is observed in other transition metal alloys (the so-called  $K$ -state alloys) and it can be explained by a modified statistics of NN atoms [19]. We note that the majority contribution is larger than the minority one for approximately  $S < 0.5$ , while opposite is true for  $S > 0.75$  and both contributions have similar values in between.

Transport vertex corrections, i.e., the vertex corrections to the Fermi-surface term, are large for small  $S$  and small for large  $S$  (Fig. 4). Interestingly, they exhibit a similar transition from large to small values like the total moment (Fig. 2). Vertex corrections, similarly as the conductivity, can be decomposed into their spin-up and spin-down parts. For spin-down channel, when the Fermi level is inside the  $d$  band, vertex corrections are small independent of the ordering. For the spin-up channel, when the Fermi energy is in the  $d$  band for well ordered samples, vertex corrections are small and comparable to spin-down counterparts. But the vertex part is increasing and large for well disordered alloy when the Fermi energy moves towards the  $sp$  band. We can conclude that the size of the vertex part (the sum of both contributions) is not primarily related to the degree of order but rather to the position of the Fermi energy with respect to the  $sp$  band.

Summarizing this part, one can say that also behavior of conductivity reflects the transition between high and low magnetic moments for  $S = 0.6$ – $0.7$ , which is related to large and very small splitting of spin-resolved DOS as discussed above.

### C. Anisotropic magnetoresistance

The anisotropic magnetoresistance (AMR) is the relativistic transport effect which can be estimated from our transport calculations (see Fig. 5). In metallic systems the AMR is typically positive so that its negative values for larger  $S$  are unusual. The negative AMR means that  $\rho_{zz}$  component becomes smaller than  $\rho_{xx} = \rho_{yy}$ . It was shown [18] that large positive values of the AMR in fcc Ni-rich alloys NiFe and NiCo are due to essentially disorder-free majority bands with very high conductivity. On the contrary, the Ni-rich NiMn alloy has disorder in both the majority and minority bands and significantly lower AMR than Ni-rich NiFe and comparable to the present case for small  $S$ . For the negative values of the AMR for large  $S$ , in particular for  $S > 0.8$ , we do not have a satisfactory explanation. We just note as the empirical fact the relation between behavior of the AMR

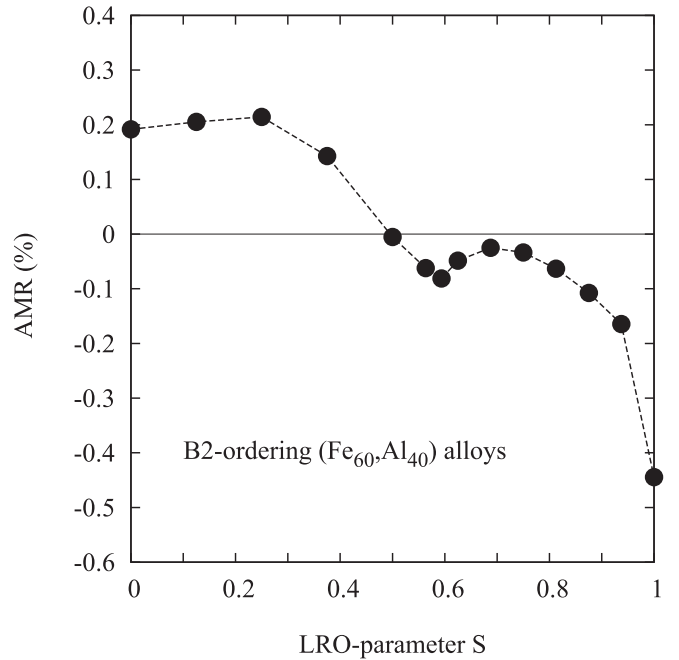


FIG. 5. Anisotropic magnetoresistance of ordering B2- ( $\text{Fe}_{60}\text{Al}_{40}$ ) alloys as a function of the LRO parameter  $S$ .

and channel conductivities (Fig. 4). Namely, for dominating majority ( $S < 0.5$ )/minority ( $S > 0.8$ ) conductivities we do have the positive/negative AMR while for  $S$  in between, where both channel conductivities are small and comparable in their values, the AMR is rather small as compared to the other two regions.

### D. Anomalous Hall effect

The important relativistic transport property is the AHC  $\sigma_{xy}$  and a closely related anomalous Hall angle  $\alpha_H = \sigma_{xy}/\sigma_{xx}$ , where  $\sigma_{xx}$  is the longitudinal conductivity. Their correct evaluation requires inclusion of both the Fermi-surface and Fermi-sea terms [11] on equal footing as shown below.

The dependence of the AHC  $\sigma_{xy}$  as a function of the order parameter  $S$  is presented in Fig. 6, together with its Fermi-sea and vertex parts. We observe a large drop of the AHC with increasing ordering at  $S \approx 0.6$  and its small values for  $S > 0.7$ . With increasing  $S$  the AHC undergoes a similar steep continuous transition as does the magnetic moment (Fig. 2), which is understandable because the AHC depends on the magnetic moment.

The Fermi-sea term is weakly changing up to the critical value of the LRO parameter ( $S \approx 0.6$ ) and for larger  $S$  it drops to small values. The Fermi-sea term is non-negligible and becomes relatively more important as  $S$  approaches the transition region. The vertex part is larger for disordered samples (small  $S$ ) as expected. It changes its sign close to the maximally ordered state similarly as in the partially ordered  $\text{L1}_0$ -FePt alloys [20]. It is also interesting to see the dependence of the AHC ( $\sigma_{xy}$ ) on the longitudinal conductivity ( $\sigma_{xx}$ ) for various values of the parameter  $S$  (Fig. 7). We clearly observe two different regimes separated by the value  $S = 0.6875$  of the order parameter  $S$  for which the  $\sigma_{xx}$  has a

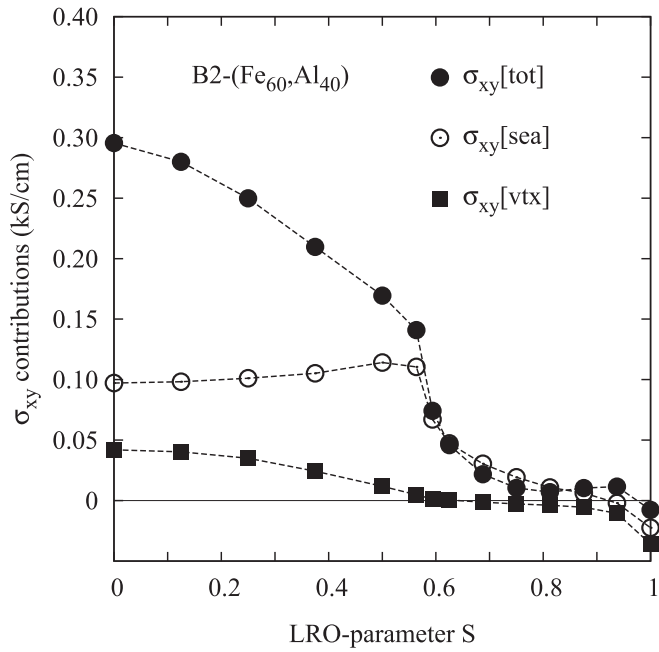


FIG. 6. Anomalous Hall conductivity  $\sigma_{xy}$  for ordering B2-(Fe<sub>60</sub>Al<sub>40</sub>) alloys as a function of the LRO parameter  $S$ . Corresponding Fermi-sea and vertex contributions are shown explicitly. Note the typical sharp transition between low and high values of  $\sigma_{xy}$  and its Fermi-sea contribution for  $S \approx 0.6$ .

minimum (see Fig. 4). Monotonically increasing dependence for disordered samples ( $S < 0.6875$ ) reflects the fact that both  $\sigma_{xy}$  and  $\sigma_{xx}$  are increasing (with decreasing  $S$ ) in this region (see Fig. 6 and Fig. 4, respectively). On the other hand, small values of  $\sigma_{xy}$  dominate behavior for ordering alloys ( $S > 0.7$ ).

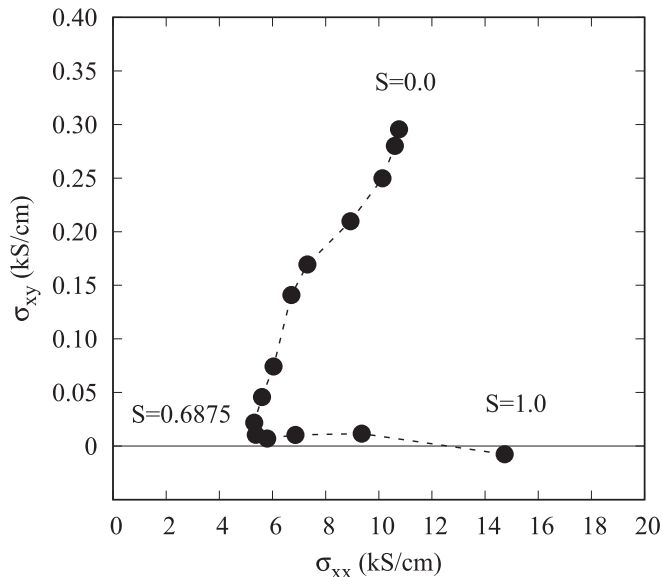


FIG. 7. Variation of  $\sigma_{xy}$  as a function of  $\sigma_{xx}$  for ordering B2-(Fe<sub>60</sub>Al<sub>40</sub>) alloys. The relevant values of  $S$  for the completely ordered alloy ( $S = 0.0$ ), the maximally ordered alloy ( $S = 1.0$ ), and alloy with the lowest  $\sigma_{xx}$  ( $S = 0.6875$ ) are shown explicitly.

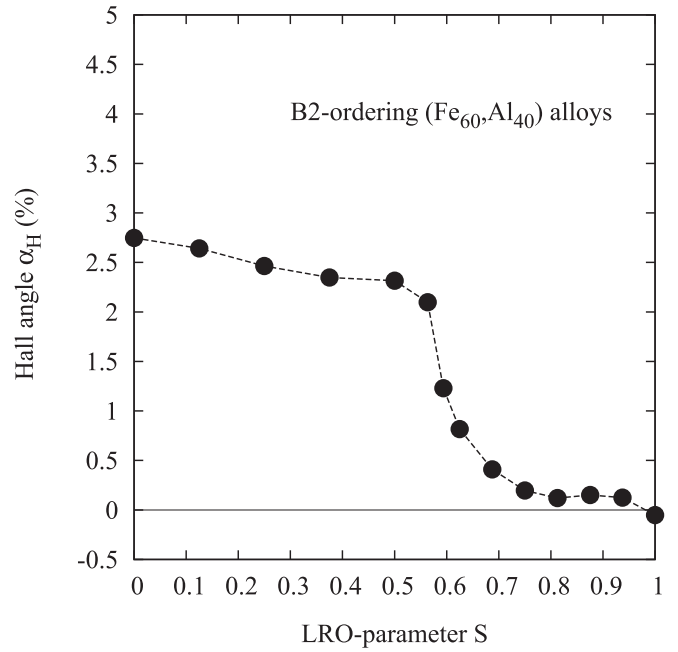


FIG. 8. Anomalous Hall angle  $\alpha_H$  of ordering B2-(Fe<sub>60</sub>Al<sub>40</sub>) alloys as a function of the LRO parameter  $S$ . Note a sharp transition between low and high values of  $\alpha_H$  for  $S \approx 0.6$ .

The most interesting result concerns the estimate of the value of the anomalous Hall angle  $\alpha_H$  due to disordering of the sample. Although our model does not assume any specific method of alloy disordering, we have implicitly in mind the ion bombardment. This means that the higher irradiation dose leads to larger disorder and vice versa. Results are shown in Fig. 8. Behavior of  $\alpha_H$  is controlled mainly by  $\sigma_{xy}$ : We obtain the same critical behavior of  $\alpha_H$  as a function of the LRO parameter  $S$  with the steep transition from large to small values of  $\alpha_H$  for  $S \approx 0.6$ . A relatively flat part for  $S < 0.6$  is a result of the competition of decreasing  $\sigma_{xy}$  and  $\sigma_{xx}$  with increasing  $S$  in this region (see Fig. 4 and Fig. 6) keeping in mind that  $\sigma_{xy}$  decreases faster. We note a very large value of  $\alpha_H$  for the present metallic system ( $\alpha_H \approx 2.75\%$ ) considering small values of the spin-orbit coupling for both Fe and Al. We note that still larger value of  $\alpha_H$  was measured for epitaxial thin film of tetragonally distorted MnGa [21]. Even more interesting is the fact that this large value is due to disordering because values of  $\alpha_H$  for well-ordered samples are negligibly small. This is due to a very small magnetic moment for such alloys as discussed above. Finally, the calculated value of  $\alpha_H$  for disordered alloy ( $S = 0$ ) agrees well with the value of 3.1% reported for a strongly irradiated (disordered) B2-(Fe<sub>60</sub>Al<sub>40</sub>) sample [7].

#### IV. CONCLUSIONS

We have studied from first principles the effect of gradual disordering from maximally ordered B2-(Fe<sub>60</sub>Al<sub>40</sub>) phase into disordered A2-(Fe<sub>60</sub>Al<sub>40</sub>) phase due to increasing amount of Fe[Al] antisites on the originally native Al sublattice. We aimed at understanding of gradual disordering of the ordered phase due to ion irradiation. We simulate disordering as a

partial long-range order with decreasing order parameter  $S$ . We found that the important role is played by the varying local environment around Fe atoms both on the native Fe and Al lattices characterized by the average number of the nearest-neighbor (NN) Fe atoms. We note that the ordered B2-(Fe<sub>60</sub>Al<sub>40</sub>) is paramagnetic at room temperature, but, as other authors, we study its ferromagnetic phase at zero temperature. The main conclusions are as follows. (i) While the local Fe[Al] moment on the native Al sublattice keeps its large value (above  $2\mu_B$ ) during the disordering process, the native local Fe[Fe] moment exhibits the transition from a large moment for the disordered phase to essentially zero moment for the well ordered phase for  $S \approx 0.6$ . We have correlated such behavior with the drop of the number of Fe-NN of Fe atoms under a certain critical value estimated to be around 3. On the other hand, the number of Fe-NN remains large and changes weakly for Fe atoms on the native Al lattice. In agreement with experiment, the disordered phase shows a pronounced ferromagnetism. (ii) The longitudinal conductivity  $\sigma_{xx}$  attains its minimum not for  $S = 0$  but for an intermediate

value of  $S$  which is related to the gradual transition of the Fermi level from the  $sp$ -like part of spectra of majority states for small  $S$  to the  $d$ -band complex with increasing  $S$ . (iii) The total AHC  $\sigma_{xy}$  reflects the critical behavior of the total magnetic moment. A similar transition from large to small values exhibits also the Fermi-sea term. (iv) The dependence of  $\sigma_{xy}$  on  $\sigma_{xx}$  clearly demonstrates different behavior of the studied alloy in regions with low and high order. (v) The most interesting result is the transition from small to large values of the anomalous Hall angle  $\alpha_H$  due to disorder. We mention in particular a large value of  $\alpha_H$  for the disordered sample (2.75%) which is close to the experimentally observed one.

### ACKNOWLEDGMENTS

The work of J.K., V.D., F.M., and I.T. was supported by a Grant No. 18-07172S from the Czech Science Foundation, F.M. acknowledges partial support from MSMT Project No. SOLID21-CZ.02.1.01/0.0/0.0/16\_019/0000760.

- 
- [1] F. Ducastelle, *Order and Phase Stability in Alloys* (North-Holland, Amsterdam, 1991).
- [2] A. Hernando, X. Amils, J. Nogués, S. Suriñach, M. D. Baró, and M. R. Ibarra, *Phys. Rev. B* **58**, R11864 (1998).
- [3] J. Sort, A. Concustell, E. Menéndez, S. Suriñach, K. V. Rao, S. C. Deevi, M. D. Baró, and J. Nogués, *Adv. Mater.* **18**, 1717 (2006).
- [4] E. Menéndez, J. Sort, M. O. Liedke, J. Fassbender, S. Suriñach, M. D. Baró, and J. Nogués, *New J. Phys.* **10**, 103030 (2008).
- [5] J. Fassbender, M. O. Liedke, T. Strache, W. Möller, E. Menéndez, J. Sort, K. V. Rao, S. C. Deevi, and J. Nogués, *Phys. Rev. B* **77**, 174430 (2008).
- [6] E. La Torre, A. Smekhova, C. Schmitz-Antoniak, K. Ollefs, B. Eggert, B. Cöster, D. Walecki, F. Wilhelm, A. Rogalev, J. Lindner, R. Bali, R. Banerjee, B. Sanyal, and H. Wende, *Phys. Rev. B* **98**, 024101 (2018).
- [7] R. Bali (private communication).
- [8] I. Turek, V. Drchal, J. Kudrnovský, M. Šob, and P. Weinberger, *Electronic Structure of Disordered Alloys, Surfaces and Interfaces* (Kluwer, Boston, 1997).
- [9] S. H. Vosko, L. Wilk, and M. Nusair, *Can. J. Phys.* **58**, 1200 (1980).
- [10] J. Kudrnovský, V. Drchal, L. Bergqvist, J. Ruzs, I. Turek, B. Újfalussy, and I. Vincze, *Phys. Rev. B* **90**, 134408 (2014).
- [11] I. Turek, J. Kudrnovský, and V. Drchal, *Phys. Rev. B* **89**, 064405 (2014).
- [12] I. Turek, J. Kudrnovský, V. Drchal, L. Szunyogh, and P. Weinberger, *Phys. Rev. B* **65**, 125101 (2002).
- [13] K. Carva, I. Turek, J. Kudrnovský, and O. Bengone, *Phys. Rev. B* **73**, 144421 (2006).
- [14] P. Mohn, C. Persson, P. Blaha, K. Schwarz, P. Novák, and H. Eschrig, *Phys. Rev. Lett.* **87**, 196401 (2001).
- [15] A. V. Smirnov, W. A. Shelton, and D. D. Johnson, *Phys. Rev. B* **71**, 064408 (2005).
- [16] G. Kresse and D. Joubert, *Phys. Rev. B* **59**, 1758 (1999).
- [17] <https://www.vasp.at>
- [18] I. Turek, J. Kudrnovský, and V. Drchal, *Phys. Rev. B* **86**, 014405 (2012).
- [19] S. Lowitzer, D. Ködderitzsch, H. Ebert, P. R. Tulip, A. Marmodoro, and J. B. Staunton, *Europhys. Lett.* **92**, 37009 (2010).
- [20] J. Kudrnovský, V. Drchal, and I. Turek, *Phys. Rev. B* **89**, 224422 (2014).
- [21] F. Wu, E. P. Sajitha, S. Mizukami, D. Watanabe, T. Miyazaki, H. Naganuma, M. Oogane, and Y. Ando, *Appl. Phys. Lett.* **96**, 042505 (2010).
- [22] J. P. Perdew, K. Burke, and M. Ernzerhof, *Phys. Rev. Lett.* **78**, 1396 (1997).